Conformational Changes in Light-Harvesting Complex II Trimer Depending on Its Binding Location

Eunchul Kim (ekim@nibb.ac.jp)
National Institute for Basic Biology
Hisako Kubota-Kawai
Yamagata University
Fumihiro Kawai
Yamagata University
Jun Minagawa
National Institute for Basic Biology

Research Article

Keywords:

Posted Date: January 24th, 2022

DOI: https://doi.org/10.21203/rs.3.rs-1258946/v1

Abstract

In green plants, the light-harvesting complex II (LHCII) trimer functions as a major antenna complex to the photosystem II (PSII) complex and a quencher to protect it from photooxidative damage. Theoretical studies on the structure of the LHCII trimer have demonstrated that excitation energy transfer between chlorophylls (Chls) can be modulated by its exquisite conformational fluctuation. However, the conformational changes in the LHCII trimer depending on its binding location have not yet been investigated, even though protein-protein interactions tend to lead conformational changes. In this study, we investigated the conformational changes in LHCII by analyzing an identical LHCII trimer comprising three different photosystem supercomplexes—PSII–LHCII supercomplexes (C_2S_2 type and $C_2S_2M_2L_2$ type) and PSI–LHCI–LHCII supercomplex—from the green alga *Chlamydomonas reinhardtii*. Consequently, the distinct differences in Chl configurations as well as polypeptide conformations of the LHCII trimers were detected based on where LHCII binds. Our analysis of the configurational factors between Chls suggests that these configurational changes lead to higher light-harvesting compatibilities in the PSII–LHCII supercomplex ($C_2S_2M_2L_2$ type) and PSI–LHCI–LHCII supercomplex. This study suggests a fine-tuned mechanism of energy transfer dynamics in LHCII trimers by regulation of protein-protein interactions.

Introduction

In green plants, chlorophyll (Chl) is the most abundant pigment that is crucially involved in photosynthesis. The first step of photosynthesis is the capture of light by Chls within the pigment-binding proteins embedded in the thylakoid membranes of chloroplasts[1]. The absorbed energy is subsequently transferred to the Chls in the reaction centers of either photosystem I or II (PSI and PSII), thereby energizing the electron transport chain from water to the Calvin-Benson cycle. The most dominant antenna protein in green plants is the light-harvesting complex II (LHCII) that contains 8 Chl *a*, 6 Chl *b*, 2 luteins, 1 violaxanthin, and 1 neoxanthin, which can efficiently harvest light in environmental light conditions. Monomeric forms of LHCII only bind to PSII, whereas its trimeric forms (LHCII trimer) bind to PSII and conditionally to PSI to balance the excitation between PSI and PSII.

Structures of the LHCII trimers from spinach have been resolved by crystallography[2,3]. These molecular structures have provided the Chl configurations that are crucial for theoretical studies of energy transfer dynamics in LHCII trimers. Theoretical analysis combined with spectroscopic analysis revealed that the Chl *a*610-*a*611-*a*612 cluster located on the outer side of the LHCII trimer exhibited predominant population of excitation energy[4–6]. Therefore, this Chl cluster has been proposed to support efficient energy transfer to the other subunits of PSII. This Chl cluster is also crucially involved in photoprotective energy dissipation[7, 8]. Moreover, Chl *a*602 and *a*603 within the stromal-side layer and Chl *a*613 within the luminal-side layer of the LHCII trimer are crucial in mediating inter-monomeric energy transfers in the LHCII trimer[9]. Furthermore, marvelous features of the LHCII trimer Chls in their electronic states have been revealed. Quantum electronic coherence in the LHCII trimer has been demonstrated by two-dimensional electronic spectroscopy with theoretical studies based on their molecular structures[10–12]. Moreover, the importance of electronic-vibrational mixing in energy transfer dynamics has been investigated by two-dimensional electronic vibrational spectroscopy[13]. In contrast, multiscale quantum mechanics/molecular mechanics (QM/MM) molecular dynamics simulations have demonstrated that the excitation energy transfer dynamics in LHCII can be modulated by its conformational fluctuation and surrounding environments including pH conditions[14–17]. These previous reports revealed that the configuration of Chls in the LHCII trimer determines their energy transfer dynamics, and therefore the eventual light-harvesting properties.

Recently, owing to the great advances in cryoelectron microscopy (cryo-EM), PSII–LHCII supercomplexes comprising the PSII core dimer and LHCII complexes (PSII–LHCII),[18–21] and the PSI–LHCI–LHCII supercomplex comprising the PSI core, LHCI, and LHCII complexes (PSI–LHCI–LHCII)[22,23] from green plants were resolved. These structures indicated that Chls in LHCII trimers are well connected to the Chls in the core complexes to ensure an efficient light-harvesting process. However, the conformation and Chl configurations of the same LHCII trimers in different supercomplexes have not yet been compared, even though protein-protein interactions can easily transform their protein and ligand structures[24, 25].

In this study, we investigated the Chl conformations in a LHCII trimer when bound to different supercomplexes. We compared the conformations of an LHCII trimer comprising identical polypeptides, namely, LhcbM1, LhcbM2, and LhcbM3 subunits with two PSII–LHCII supercomplexes—C_2S_2 and $C_2S_2M_2L_2$— and a PSI–LHCI–LHCII supercomplex from a green alga *Chlamydomonas reinhardtii* (*C. reinhardtii*) (Figure 1A) (Table S1)[20, 23]. Moreover, to quantify the difference in the Chl configurations, computational analysis was

applied to determine the distances and orientation factors between all Chl based on estimated transient dipoles. The effects of the configurational change on site energy and energy transfer dynamics were estimated by calculating energy transfer rate constants based on the Förster resonance energy transfer principle. Based on these results, we propose the way how energy transfer dynamics on LHCII can be modulated by its binding partners.

Results

Conformations of LHCII trimers in three different photosystem supercomplexes

In order to investigate whether the structure of the same LHCII trimer can be affected by where it binds, the polypeptide structures and Chl coordinates of an LHCII trimer comprising LhcbM1, LhcbM2, and LhcbM3 were compared with the two PSII–LHCII supercomplexes—C_2S_2 and $C_2S_2M_2L_2$— and the PSI–LHCI–LHCII supercomplex from a green alga *C. reinhardtii* (Figure 1A). The S-trimer in the C_2S_2 supercomplex (pdb.6KAC) is a hetero trimer of LHCII comprising LhcbM1, LhcbM2, and LhcbM3[20]. Although the polypeptide identities have not been reported in the $C_2S_2M_2L_2$ supercomplex (pdb.6KAD) because of low resolution around the S-trimer region[20], we assume its S-trimer is also comprises LhcbM1, LhcbM2, and LhcbM3, as in the C_2S_2 supercomplex. The LHCII-1 trimer in the PSI–LHCI–LHCII supercomplex (pdb.7DZ7) has been reported to be the same hetero trimer, namely, LhcbM1/LhcbM2/LhcbM3[23]. In all three locations, the LhcbM1/LhcbM2/LhcbM3 trimer binds to a core complex with LhcbM1 as the docking site (Figure 1A). The superposed polypeptide structures revealed that the polypeptide structure of the LHCII trimer was not identical when bound to the different supercomplexes (Figure 1B). The S-trimer bound to PSII $C_2S_2M_2L_2$ is slightly stretched to the outside, while the central part stays the same. Similarly, Chls in the S-trimer/$C_2S_2M_2L_2$ are stretched out unlike those in the S-trimer/C_2S_2 or LHCII-1/PSI–LHCI–LHCII supercomplexes (Figure 1C). This clearly suggests that both the polypeptide structure and the Chl coordinates in an LHCII trimer can vary depending on where it binds.

In order to investigate the flexible domain of the LHCII trimer affected by vicinity, we analyzed the root mean square deviation (RMSD) of the polypeptides between each photosystem supercomplex (Figure 2). Our analysis revealed that the polypeptide conformation of the S-trimer/$C_2S_2M_2L_2$ is considerably different compared to the S-trimer/C_2S_2 and LHCII-1/PSI–LHCI–LHCII supercomplexes, whereas there was no significant difference between S-trimer/C_2S_2 and LHCII-1/PSI–LHCI–LHCII supercomplexes (Figure 2A). In the RMSD map between S-trimer/C_2S_2 and S-trimer/$C_2S_2M_2L_2$, the lumen side of helix B of all LhcbM and helix C/LhcbM2 exhibited high RMSD values. In the RMSD map between S-trimer/$C_2S_2M_2L_2$ and LHCII-1/PSI–LHCI–LHCII, helix C of all LhcbM, helix A of LhcbM2 and LhcbM3, and helix B exposed to the lumen sides of LhcbM2 and LhcbM3 revealed high overall RMSD values. In contrast, the RMSD map between S-trimer/C_2S_2 and LHCII-1/PSI–LHCI–LHCII revealed lower RMSD values except for the stroma sides of helix A of LhcbM2 and LhcbM3. Figure 2B displays the placements of Chls and carotenoids on the RMSD map between the S-trimer/$C_2S_2M_2L_2$ and LHCII-1/PSI–LHCI–LHCII.

Chls configurations in LHCII trimers of three different photosystem supercomplexes

In order to examine the positional effects on Chl configurations, we superimposed the PDB coordinates and the corresponding electron density maps of a low-energy Chl *a*611-*a*612 pair located between helix A and neighbor helix C, in each LHCII subunit of the three different photosystem supercomplexes and displayed their corresponding cryo-EM maps (Figure3). In LhcbM1,as the RMSD values were found to be low, the relative configuration of the Chl pair and its cryo-EM maps were also found to be analogous. In contrast, in LhcbM2 and LhcbM3, the RMSD values of helix A and helix C were found to be high; therefore, the relative configurations of the Chl pair and the cryo-EM maps differed between photosystem supercomplexes.

Configurational factors such as distance and orientation factors between transient dipole moments of Chls are critical factors for excitation energy transfer dynamics. A weaker dipole interaction induced by a long distance or low orientation factor can result in a lower energy transfer rate. Therefore, we conducted computational analysis for distances and orientation factors between all transient dipole moments of Chls to quantify the effects of different Chl coordinates on Chl configuration. The distance between the central magnesium atoms of the porphyrin rings in Chls was used to calculate the distances and the three-dimensional angles between the unit vectors that were generated based on the coordinates of NB and ND atoms of the porphyrin rings in Chls[20, 26]. Our

comparative analysis clearly indicates that Chl configurations in LHCII trimers are modulated by the polypeptides in the vicinity (Figure 4A), suggesting that the energy transfer properties of the LHCII trimer could be modulated by its binding parter.

In order to estimate the impact of Chl configuration change in the LHCII trimers upon excitation energy transfer dynamics, "interaction factor" was calculated as the energy transfer rate based on the Förster resonance energy transfer (FRET) principle (Figure 4B). In all LHCII subunits, the Chl *a*611 and *a*612 pair exhibited the highest interaction factor because of their high orientation factor and relatively short distance (Table 1). Consistent with literature, Chl *a*611, *a*612, and *a*610 were found to be in their lowest energy states because of their strong coupling interactions[4, 5]. Our results revealed that the interaction factors of the Chl *a*611-*a*612 pairs were different in LhcbM2 and LhcbM3, whereas these were similar in LhcbM1 between the three different supercomplexes. In LhcbM2 the interaction factors of the Chl *a*611-*a*612 pairs in PSII $C_2S_2M_2L_2$ and PSI–LHCI–LHCII were 21 and 14% lower than that in PSII C_2S_2, respectively. In LhcbM3, the interaction factors of the Chl *a*611-*a*612 pairs in PSII $C_2S_2M_2L_2$ and PSI–LHCI–LHCII were 11 and 13% lower than that in PSII C_2S_2, respectively. Furthermore, the closest Chl pair—*b*606-*a*604—exhibited apparent changes depending on where the LHCII binds. The distance between the Chl *b*606-*a*604 pair in LhcbM2 was found to be longer in $C_2S_2M_2L_2$ than that in C_2S_2 and PSI–LHCI–LHCII.

Table 1. interaction factors between Chl pairs. Significant differences compared to PSII C_2S_2 are indicated by asterisks. (* > 10% difference, ** > 20% difference, *** > 40%)

Chl pair	C_2S_2			$C_2S_2M_2L_2$			PSI–LHCI–LHCII			
	LhcbM1	**LhcbM2**	**LhcbM3**	**LhcbM1**	**LhcbM2**	**LhcbM3**	**LhcbM1**	**LhcbM2**	**LhcbM3**	
Chl a611-a612	**interaction factor**	16.68	16.78	16.59	16.25	13.21**	14.77*	16.66	14.50*	14.48*
	Distance	9.57	9.50	9.57	9.64	9.60	9.84	9.45	9.66	9.66
	Orientation factor	2.29	2.20	2.28	2.33	1.85*	2.39	2.12	2.11	2.11
Chl a610-a612	**interaction factor**	0.62	0.73	0.51	0.70*	0.38***	0.55	0.64	0.34***	0.28***
	Distance	11.56	12.06	11.93	11.90	12.21	12.01	11.71	11.99	12.06
	Orientation factor	0.26	0.40	0.26	0.35*	0.22***	0.30*	0.30	0.18***	0.16**
Chl a610-a611	**interaction factor**	0.60	0.55	0.62	0.56	0.46*	0.53*	0.65	0.57	0.57
	Distance	17.74	18.09	17.77	17.93	18.47	18.31	17.58	17.91	17.92
	Orientation factor	3.34	3.48	3.51	3.34	3.25	3.54	3.42	3.37	3.38
Chl a613-a614	**interaction factor**	2.91	2.92	2.65	1.62***	2.79	2.79	2.75	3.40*	3.40**
	Distance	9.32	9.35	9.45	9.60	9.56	9.61	9.47	9.64	9.64
	Orientation factor	0.34	0.35	0.34	0.23**	0.38	0.39**	0.36	0.49***	0.49***
Chl a602-a603	**interaction factor**	1.03	1.03	1.02	0.59***	0.66**	0.82**	0.76**	0.92*	0.87*
	Distance	11.68	11.66	11.80	11.92	12.04	11.98	11.55	11.58	11.64
	Orientation factor	0.47	0.46	0.49	0.30**	0.36**	0.44*	0.32**	0.40*	0.39*

Furthermore, we compared the interaction factors of the other Chl pairs of low energy Chls— the Chl *a*610-*a*612 pair and the Chl *a*610-*a*611 pair— (Table 1). Interestingly, the Chl *a*610-*a*612 pair was found to be significantly different in LhcbM2 of PSII $C_2S_2M_2L_2$ (LhcbM2/$C_2S_2M_2L_2$), LhcbM2/PSI–LHCI–LHCII, and LhcbM3/PSI–LHCI–LHCII. The interaction factors of the Chl *a*610-*a*612 pairs in LhcbM2/$C_2S_2M_2L_2$ and LhcbM2/PSI–LHCI–LHCII were 48 and 53% lower than that in the LhcbM2/C_2S_2, respectively, mostly because of lower orientation factors (45 and 55% lower, respectively). However, the interaction factors of Chl *a*610-*a*612 pairs in LhcbM3/$C_2S_2M_2L_2$ and LhcbM3/PSI–LHCI–LHCII were 8% higher and 45% lower than that in LhcbM3/C_2S_2. Moreover, the interaction factors of the Chl *a*610-*a*611 pairs in LhcbM2 and LhcbM3 of PSII $C_2S_2M_2L_2$ were 16 and 15% lower than those in PSII C_2S_2, respectively, whereas there were no significant differences between PSII C_2S_2 and PSI–LHCI–LHCII.

Although intra-LHCII energy transfer is important for fast energy transfer dynamics, inter-LHCII energy transfer is also crucial as an efficient antenna complex for photosystem core complexes. Here, we investigated the Chl configurations at the interface of the LHCII subunits in the LHCII trimer of the three different photosystem supercomplexes. As shown in the Chl configurations within each LHCII subunit (Figure 3A), Chl configurations between LHCII subunits also varied depending on the vicinity and type of LHCII subunits (Figure 4C). The closest Chls between the LHCII subunits were Chl *b*601 and *b*609 in all LhcbM interfaces. However, Chl *b* rapidly transfers excitation energy to Chl *a* and the reverse transfer rarely occurs because of the higher energy level of Chl *b* than that of Chl *a*; therefore, Chl *b*601 and *b*609 are unable to function as major mediators for inter-LHCII energy transfer. We thus focused on the Chl *a* pairs that are mainly involved in inter-LHCII energy transfer. Consistent with the previous study[9], our results showed that Chl *a*602-*a*603, Chl *a*603-*a*603, and Chl *a*603-*a*613 pairs have higher interaction factors at all LhcbM interfaces (Figure 4D). At the LhcbM1-LhcbM2 interface, the interaction factor of the Chl *a*602-*a*603 in PSII $C_2S_2M_2L_2$ was found to be higher than those in PSII C_2S_2 and PSI–LHCI–LHCII. In contrast, at the LhcbM1-LhcbM3 interface, the interaction factor of the Chl *a*602-*a*603 in PSII $C_2S_2M_2L_2$ was found to be lower than those in PSII C_2S_2 and PSI–LHCI–LHCII. This result indicates that energy transfer between LhcbM1 and LhcbM2 is enhanced; however, energy transfer between LhcbM1 and LhcbM3 is suppressed in PSII $C_2S_2M_2L_2$ compared to those in PSII C_2S_2 and PSI–LHCI–LHCII. At the LhcbM2-LhcbM3 interface, although the interaction factor of the Chl *a*602-*a*603 pair in PSII $C_2S_2M_2L_2$ was similar to those in PSII C_2S_2 and PSI–LHCI–LHCII, the interaction factors of the Chl *a*603-*a*603 pairs were largely increased in PSII C_2S_2 and PSI–LHCI–LHCII, but not in PSII $C_2S_2M_2L_2$. This result suggests that energy transfer mediated by the Chl *a*602-*a*603 pair between LhcbM2 and LhcbM3 is more active in PSII C_2S_2 and PSI–LHCI–LHCII than in PSII $C_2S_2M_2L_2$. Furthermore, we investigated the interaction factors between Chl *a*603 and other Chls within the LHCII subunit (Table 1), where Chl *a*603 is supposed to be important in inter-LHCII energy transfer[4]. Consistently, Chl *a*603 revealed the highest interaction factor with Chl *a*602 within the overall LHCII subunit. Interestingly, the interaction factors of the Chl *a*602-*a*603 pair in PSII C_2S_2 were higher than those in PSII $C_2S_2M_2L_2$ and PSI–LHCI–LHCII mainly because higher orientation factor values in all LhcbM subunits.

The crystal structures of the vascular plant LHCII trimer have been resolved[3, 28]. Notably, the crystallized LHCII trimer has been reported to exhibit a photoprotective-dissipation state[7]. Therefore, we compared the Chl configurations in the LHCII trimers amongst the crystallized LHCII trimer, LHCII trimers in PSII–LHCII supercomplexes (C_2S_2[18] and $C_2S_2M_2$[19]), and PSI–LHCI–LHCII[22] to examine the change(s) responsible for inducing the quenching state of LHCII (Figure S1A) (Table S2). Because each LHCII subunit of the plant LHCII trimer has not been completely identified, the respective LHCII subunits were compared based on the locations of the LHCII trimers in *C. reinhardtii* whereas LHCII subunits of crystalized LHCII trimers were not classified due to its uncertainty. The distance and orientation factor of each Chl pair in each LHCII subunit are shown in Figure S1B. In all LHCII subunits, Chl configurations varied in crystallized LHCII trimers and in different photosystem supercomplexes. Furthermore, symmetric LHCII subunits in the 3 LHCII trimers of the LHCII crystal were observed. We compared the interaction factors based on the FRET principle to estimate the effect of the change in Chl configurations in the LHCII trimers (Figure S1C). Interestingly, Chl *a*611-*a*612 pairs in the LHCII-i and LHCII-iii subunits of the crystallized LHCII trimer exhibited ~25% lower interaction than those of PSII–LHCII and PSI–LHCI–LHCII supercomplexes, whereas Chl *a*611-*a*612 pairs in LHCII-ii of both the crystallized LHCII and the PSI–LHCI–LHCII supercomplex exhibited ~25% lower interaction factors than those of the PSII–LHCII supercomplexes. In contrast, Chl *b*606-*a*604 pairs in the LHCII-i and LHCII-iii subunits of the crystallized LHCII trimer and the PSI–LHCI–LHCII supercomplex had a longer distance than those of the PSII–LHCII supercomplexes. For the LHCII-ii, the Chl *b*606-*a*604 pair in the crystallized LHCII trimer exhibited a longer distance than those of the PSII–LHCII and PSI–LHCI–LHCII supercomplexes. These results indicate that the Chl *a*611-*a*612 pair in LHCII-ii is analogous between the crystallized LHCII and the PSI–LHCI–LHCII supercomplex, whereas the Chl *b*606-*a*604 pair in the LHCII-i and LHCII-iii are analogous between the crystallized LHCII and the PSI–LHCI–LHCII supercomplex. These results indicate that

configurational change in the low-energy Chl cluster may be responsible for switching between the light-harvesting and photoprotective states of LHCII.

Discussion

Comparative analysis of the molecular structures of the photosystem supercomplexes revealed that the polypeptide structures and Chl coordinates of the LHCII trimer are flexible based on where the LHCII trimer binds. Quantitative comparisons of the configurational factors and estimation of the interaction factors between Chl pairs demonstrate that these flexible Chl configurations can significantly affect the energy transfer dynamics in LHCII. These results imply a regulation mechanism of the light-harvesting system by modulating protein-protein interactions, as reported previously for the array formation of PSII–LHCII supercomplexes[27] and aggregation of the LHCII trimers[29]. We expect that this mechanism enables green algae to modulate the light-harvesting system according to the environmental factors, such as intensity as well as quality of light, and the redox state of the electron acceptor pool.

Our analysis revealed that notable changes occur in the *a*610-*a*611-*a*612 cluster, which is an important low-energy Chl cluster, because of its strong coupling interactions in LHCII[4,5,9]. This Chl cluster has the lowest site energy; therefore, the excitation energy has been known to be predominantly localized in this cluster. Moreover, this cluster is proposed to transfer the excitation energy to the excited state of the low-lying carotenoid, Lutein-1[7, 8], which is in a photoprotective-dissipation state. We therefore propose that a configurational change in the low-energy Chl cluster switches the light-harvesting and photoprotective modes of LHCII. Our results demonstrated that the configurational factors of Chl *a*611-*a*612 and Chl *a*610-*a*612 are significantly altered, whereas those of Chl *a*610-*a*611 were not (Table 1). This result indicates that Chl *a*612 plays a pivotal role to control the excitation energy transfer dynamics in LHCII. Comparison of the LHCII subunits in the LHCII trimer also revealed that changes occur in outer LHCII subunits, LhcbM2 and LhcbM3, rather than in the inner LHCII subunit, LhcbM1. A decrease in interaction factors between Chl pairs implicate weaker coupling interactions resulting in a higher site energy than that of strong coupling interactions. This can ensure that the energy localization effect is smaller in outer LHCII subunits; therefore, it increases energy transfer efficiency to the core complexes in PSII $C_2S_2M_2L_2$ and PSI–LHCI–LHCII.

The other notable change was observed in the closest Chl pair *b*606-*a*604, which functions as an energy transmitter among the LHCII subunits in the LHCII trimer[9]. Therefore, longer distances between the Chl pair *b*606-*a*604 can affect the inter-monomer energy transfer. We postulate that the inter-LHCII energy transfer from LhcbM2 to other LHCII subunits is inhibited such that external energy transfer from the S-LHCII trimer to M-LHCII trimer is promoted in $C_2S_2M_2L_2$, as previously proposed by Sheng *et al.*[20]. Therefore, we propose that the formation of $C_2S_2M_2L_2$ under low-light conditions increases the light-harvesting capability, and formation of C_2S_2 under high-light conditions suppresses the light-harvesting capability, thereby inhibiting over-excitation at the core complexes.

Our comparative analysis on vascular plant LHCII trimers demonstrated that Chl configurations in the crystalized LHCII trimers, which is regarded as photoprotective-dissipation state LHCII trimers[7], were distinct from that in PSII–LHCII and PSI–LHCI–LHCII supercomplexes. Notably, Chl *a*611-*a*612 and Chl *b*606-*a*604 pairs showed significant difference, which were the lowest energy site and an energy transmitter among the LHCII subunits in the LHCII trimers. These differences are supposed to lead changes in excitation energy transfer dynamics in the LHCII trimers. We regard these changes in Chl configurations act as a switch between light-harvesting and photoprotective dissipation states of the LHCII trimers. To prove it, further structural analysis to exclude the effect by the observation methods (cryo-EM vs. crystallography) to the conformational change and theoretical studies to investigate the energy transfer dynamics would be required.

Finally, we would like to highlight our findings about the molecular structures of photosystem supercomplexes. We propose that the light-harvesting efficiency by the LHCII trimer is higher in PSII–LHCII $C_2S_2M_2L_2$ and PSI–LHCI–LHCII supercomplexes but lower in PSII–LHCII C_2S_2 supercomplex due to the conformational changes of the LHCII trimer. In this study, we present relatively large structural differences rather than finer structural differences; however, it would be necessary to determine the precise Chl coordinates for further quantum mechanical analysis of energy transfer dynamics, which require higher spatial resolution of the structural data. Moreover, the possibility that the Chl coordinates in LHCII within the biochemical samples, such as supercomplexes, can be affected by detergents or buffer conditions during sample preparation. Although we compared LHCII trimers in the same buffer conditions in this study (Table S1), the effect of buffer conditions on the conformation and Chl configuration of the LHCII trimer should be studied

carefully and systematically. The details of energy transfer dynamics remain to be studied by multiscale quantum mechanics/molecular mechanics (QM/MM) molecular dynamics simulations on these conformational changes in LHCII trimers.

Materials And Methods

Superposition and RMSD calculations using PDB data

Protein data bank (PDB) data listed in Table S1 and S2 were used in this study. Superposition of polypeptides structures and Chl *a*611-*a*612 pairs of LhcbM1 (6kac chain Y, 6kad chain Y, 7dz7 chain Z), LhcbM2 (6kac chain G, 6kad chain G, 7dz7 chain X), and LhcbM3 (6kac chain N, 6kad chain G, 7dz7 chain Y) were performed using the Pair fitting function of Pymol (PyMOL(TM) Molecular Graphics System, Version 1.8.6.0. Schrodinger, LLC.) with magnesium atoms and NA, NB, NC, ND atoms of the porphyrin rings of the Chls. Least square comparison of LHCII trimer structures and calculation of the root-mean-square deviations (RMSD) of the Cα atoms were performed by LAQKAB in CCP4[30]. The color-coded LHCII structures for the RMSD values were represented by Pymol.

Computational analysis of configurational factors and FRET rate constants

In order to estimate the configurational factors, we applied a customized algorithm on the Python platform (Python v.3.6) [26]. As an interaction factor for the impact of configurational changes in Chl pairs, FRET rate constants were calculated based on FRET theory. The FRET rate constants (k_{FRET}) were defined as $k_{FRET} = (C\kappa^2)/(n^4R^6)$; where, C is the factor calculated from spectral overlap integral between the two Chls, κ^2 is the dipole orientation factor, n is the refractive index, and R is the distance between two Chls. The applied C values for Chl *a*→Chl *a*, Chl *a*→Chl *b*, Chl *b*→Chl *a*, and Chl *b*→Chl *b* were 32.26, 1.11, 9.61 and 14.45, respectively; these values were estimated by Gradinaru *et al*. [31]. κ^2 was defined as $\kappa^2 = [\hat{u}_D \cdot - - 3(\hat{u}_D \cdot \hat{R}_{DA})(\hat{u}_A \cdot \hat{R}_{DA})]^2$; where $\hat{u}_D$ and $\hat{u}_A$ are the dipole unit vectors of donor and acceptor Chls derived using the vectors from the coordinates of NB and ND atoms, $\hat{R}_{DA}$ and is the unit vector of the vector originating from the magnesium of the donor Chl to the magnesium of the acceptor Chl. The value of n was 1.55. R was taken from the distance between central magnesium atoms of the two Chls. FRET rates were computationally calculated using a customized algorithm on the Python platform (Python v.3.6). For S-trimers of PSII–LHCII supercomplexes (6kac, 6kad, 3jcu, and 5xnl), configuration factors, and interaction factors from two S-trimers were determined. For crystallized LHCII trimers (1rwt), configuration factors and interaction factors from all three LHCII trimers were indicated.

Declarations

Acknowledgements

We thank Prof. Akihito Ishizaki and Dr. Makio Yokono for helpful discussion. This work was supported by Grant-in-Aid from the Japan Society for the Promotion of Science (JSPS) (JP21K15129 for E.K and JP20K06502 for H.K.-K.), Takeda Science Foundation for E.K, and 2021 Yamagata University – Center Of Excellence (Collaboration) (YU-COE(C)) program Yamagata University Carbon Neutral Research Center (YUCaN) for H.K.-K.

Author contributions

E.K., H.K.-K, F.K., and J.M. conceived and designed the research. H.K.-K. and F.K. conducted comparison analyses of polypeptide structures, chlorophylls, and electron density maps. E.K. performed computational calculations for configurational factors and interaction factors between chlorophylls. E.K. curated the data and wrote the initial draft of the manuscript. J.M. provided supervision and revised the manuscript. All authors contributed to revising the manuscript and approve the final version of the manuscript.

Competing Interests Statement

The authors declare no competing interests.

References

1. Blankenship, R. E. *Molecular mechanisms of Photosynthesis*. (Blackwell Science, 2002).
2. Liu, Z. F. *et al.* Crystal structure of spinach major light-harvesting complex at 2.72 angstrom resolution. Nature **428**, 287–292, doi:Doi 10.1038/Nature02373 (2004).
3. Standfuss, J., van Scheltinga, A. C. T., Lamborghini, M. & Kühlbrandt, W. Mechanisms of photoprotection and nonphotochemical quenching in pea light-harvesting complex at 2.5 Å resolution. EMBO J. **24**, 919–928 (2005).
4. Novoderezhkin, V. I., Palacios, M. A., van Amerongen, H. & van Grondelle, R. Excitation dynamics in the LHCII complex of higher plants: Modeling based on the 2.72 Å crystal structure. J. Phys. Chem. B **109**, 10493–10504 (2005).
5. Schlau-Cohen, G. S. *et al.* Pathways of energy flow in LHCII from two-dimensional electronic spectroscopy. J. Phys. Chem. B **113**, 15352–15363 (2009).
6. Renger, T. Theory of excitation energy transfer: from structure to function. Photosynth. Res. **102**, 471–485 (2009).
7. Pascal, A. A. *et al.* Molecular basis of photoprotection and control of photosynthetic light-harvesting. Nature **436**, 134–137 (2005).
8. Ruban, A. V. *et al.* Identification of a mechanism of photoprotective energy dissipation in higher plants. Nature **450**, 575–578 (2007).
9. Novoderezhkin, V., Marin, A. & van Grondelle, R. Intra- and inter-monomeric transfers in the light harvesting LHCII complex: The Redfield-Förster picture. Phys. Chem. Chem. Phys. **13**, 17093–17103 (2011).
10. Ishizaki, A. & Fleming, G. R. Quantum coherence in photosynthetic light harvesting. Annu. Rev. Condens. Matter Phys. **3**, 333–361 (2012).
11. Schlau-Cohen, G. S. *et al.* Elucidation of the timescales and origins of quantum electronic coherence in LHCII. Nat. Chem. **4**, 389–395 (2012).
12. Ishizaki, A. & Fleming, G. R. Theoretical examination of quantum coherence in a photosynthetic system at physiological temperature. *Proc. Natl. Acad. Sci. U. S. A.* **106**, 17255–17260 (2009).
13. Arsenault, E. A., Yoneda, Y., Iwai, M., Niyogi, K. K. & Fleming, G. R. Vibronic mixing enables ultrafast energy flow in light-harvesting complex II. Nat. Commun. **11**, 1460 (2020).
14. Liguori, N., Periole, X., Marrink, S. J. & Croce, R. From light-harvesting to photoprotection: structural basis of the dynamic switch of the major antenna complex of plants (LHCII). Sci Rep-Uk **5**, 15661 (2015).
15. Balevicius, V. *et al.* Fine control of chlorophyll-carotenoid interactions defines the functionality of light-harvesting proteins in plants. Sci Rep-Uk **7**, 13956 (2017).
16. Daskalakis, V. *et al.* Structural basis for allosteric regulation in the major antenna trimer of photosystem II. J. Phys. Chem. B **123**, 9609–9615 (2019).
17. Cupellini, L., Bondanza, M., Nottoli, M. & Mennucci, B. Successes & challenges in the atomistic modeling of light-harvesting and its photoregulation. Biochim. Biophys. Acta - Bioenerg. **1861**, 148049 (2020).
18. Wei, X. *et al.* Structure of spinach photosystem II-LHCII supercomplex at 3.2 Å resolution. Nature **534**, 69–74 (2016).
19. Su, X. D. *et al.* Structure and assembly mechanism of plant C2S2M2-type PSII-LHCII supercomplex. Science **357**, 815–820 (2017).
20. Sheng, X. *et al.* Structural insight into light harvesting for photosystem II in green algae. Nat. Plants **5**, 1320–1330 (2019).
21. Shen, L. L. *et al.* Structure of a C2S2M2N2-type PSII–LHCII supercomplex from the green alga *Chlamydomonas reinhardtii*. *Proc. Natl. Acad. Sci. U. S. A.* **116**, 21246–21255 (2019).
22. Pan, X. W. *et al.* Structure of the maize photosystem I supercomplex with light-harvesting complexes I and II. Science **360**, 1109–1112 (2018).
23. Pan, X. W. *et al.* Structural basis of LhcbM5-mediated state transitions in green algae. Nat. Plants **7**, 1119–1131 (2021).
24. Nooren, I. M. A. & Thornton, J. M. Structural characterisation and functional significance of transient protein-protein interactions. J. Mol. Biol. **325**, 991–1018 (2003).
25. Nooren, I. M. A. & Thornton, J. M. Diversity of protein-protein interactions. EMBO J. **22**, 3486–3492 (2003).
26. Kim, H., Kim, E., Vargas, M. & Minagawa, J. Photosystem II network benefits from mixed chlorophylls in the antennae. arXiv, arXiv:2101.04848 [physics.data-an] (2021).

27. Kim, E., Watanabe, A., Duffy, C. D. P., Ruban, A. V. & Minagawa, J. Multimeric and monomeric photosystem II supercomplexes represent structural adaptations to low- and high-light conditions. J. Biol. Chem. **295**, 14537–14545, doi:10.1074/jbc.RA120.014198 (2020).
28. Liu, Z. F. *et al.* Crystal structure of spinach major light-harvesting complex at 2.72 Å resolution. Nature **428**, 287–292 (2004).
29. Kim, E., Kawakami, K., Sato, R., Ishii, A. & Minagawa, J. Photoprotective Capabilities of Light-Harvesting Complex II Trimers in the Green Alga Chlamydomonas reinhardtii. J. Phys. Chem. Lett. **11**, 7755–7761, doi:10.1021/acs.jpclett.0c02098 (2020).
30. Kabsch, W. A solution for the best rotation to relate two sets of vectors. Acta Crystallogr. A. **32**, 922–923 (1976).
31. Gradinaru, C. C. *et al.* The flow of excitation energy in LHCII monomers: Implications for the structural model of the major plant antenna. Biophys. J. **75**, 3064–3077 (1998).

Figures

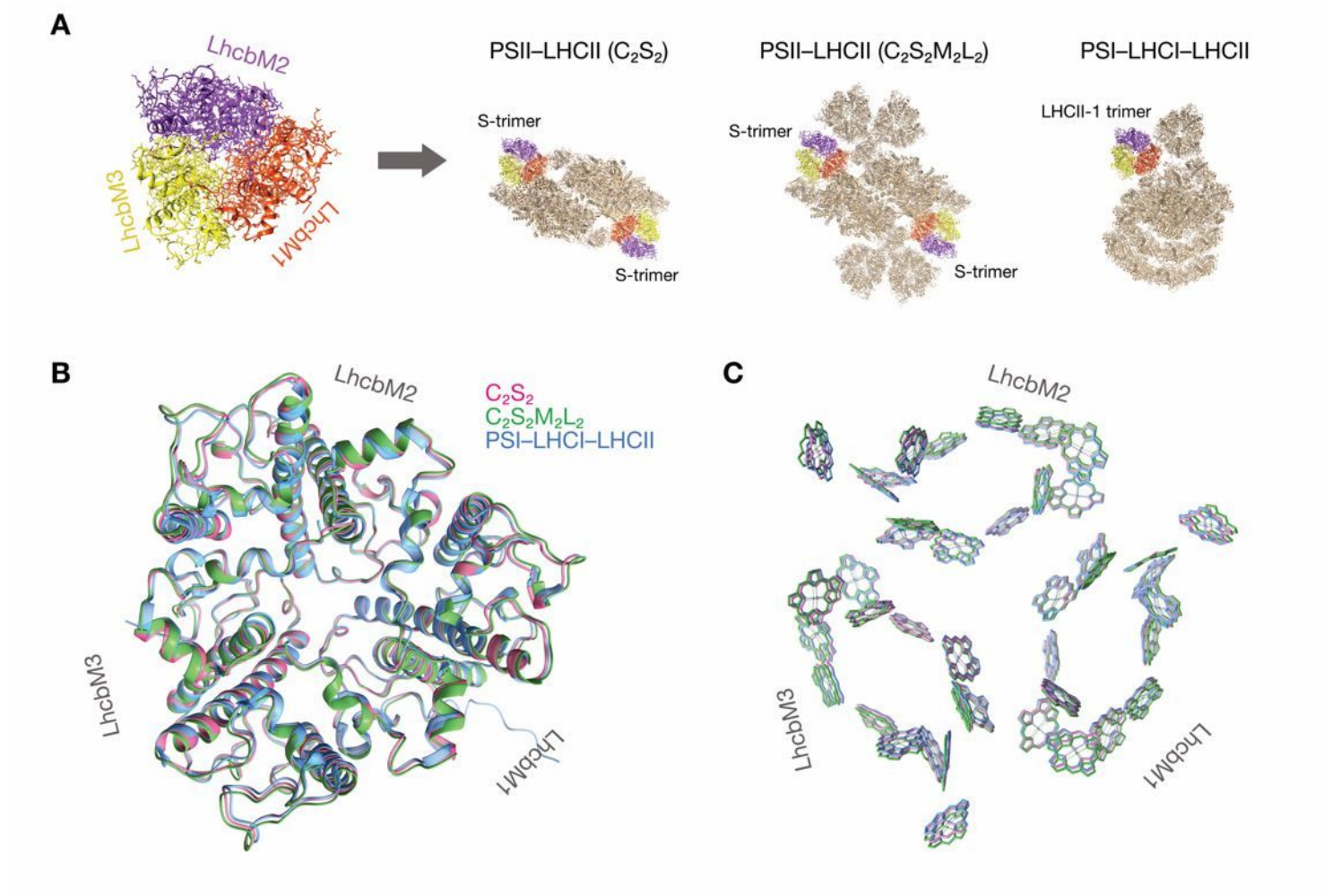

Figure 1

Conformations of LHCII trimers in three different photosystem supercomplexes. (A) LHCII trimer comprising LhcbM1, LhcbM2, and LhcbM3, and the locations of the LHCII trimers in PSII–LHCII supercomplexes—C_2S_2 (pdb.6kac) and $C_2S_2M_2L_2$ (pdb.6kad)—and a PSI–LHCI–LHCII supercomplex (pdb.7dz7) from a green alga *C. reinhardtii*. LhcbM1, LhcbM2, and LhcbM3 are represented by orange, purple, and yellow colors, respectively. (B) Superposed polypeptide structures and (C) superposed image of porphyrin rings of Chls in the LHCII trimers of the three different photosystem supercomplexes. LHCII trimers from C_2S_2, $C_2S_2M_2L_2$, and PSI–LHCI–LHCII supercomplexes are represented by pink, green, and cyan colors, respectively.

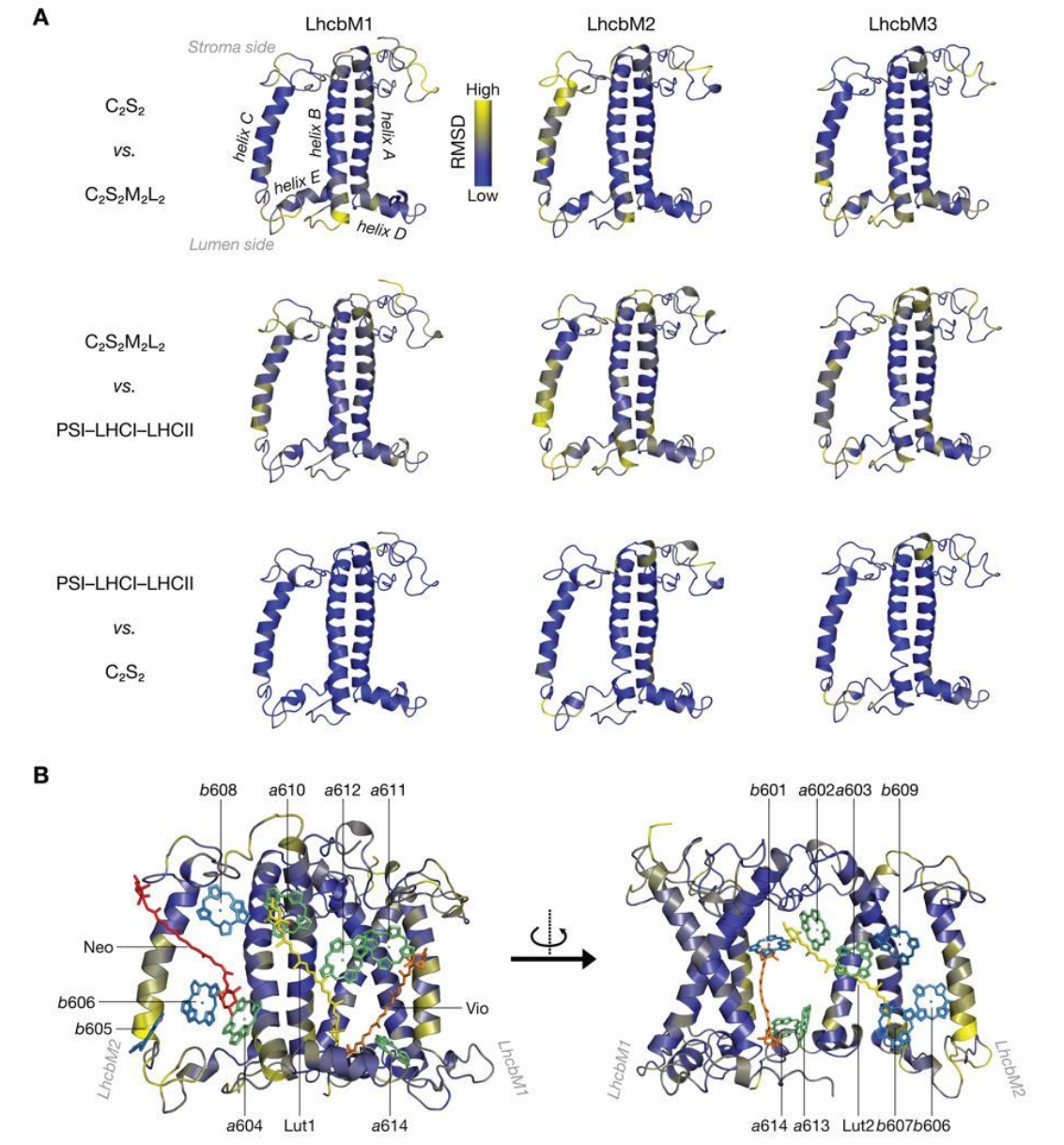

Figure 2

Conformational differences between the LHCII trimers. (A) Polypeptide structures of LHCII subunits, color-coded for the root mean square deviation (RMSD) values from C_2S_2 vs. $C_2S_2M_2L_2$, $C_2S_2M_2L_2$ vs. PSI–LHCI–LHCII, and PSI–LHCI–LHCII vs. C_2S_2. RMSD values are indicated with colors ranging from blue (identical) to yellow (different, >2.0Å). (B) Two different side-views of the LhcbM2-LhcbM1, color-coded for the RMSD values from $C_2S_2M_2L_2$ vs. PSI–LHCI–LHCII, with placements of Chls and carotenoids.

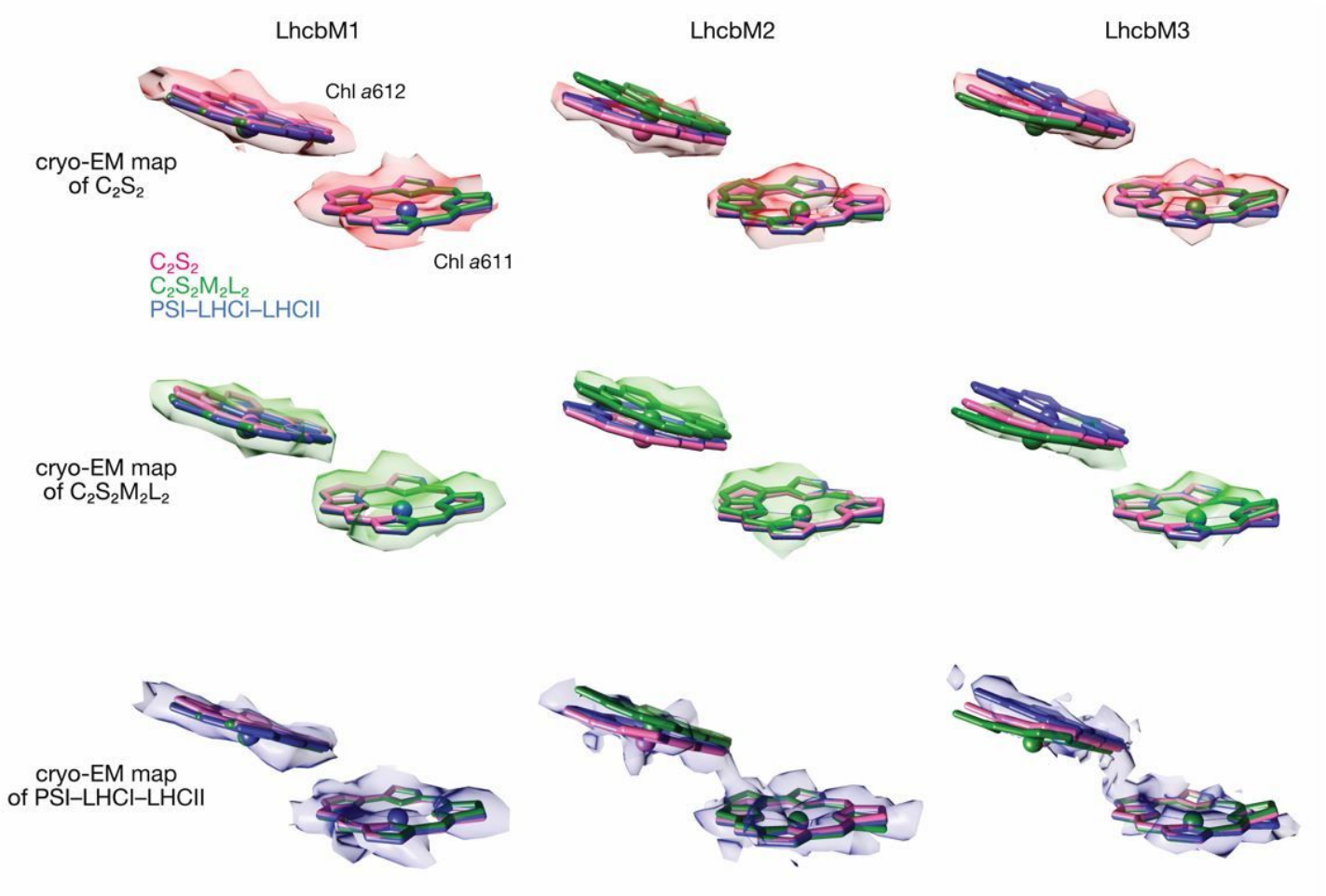

Figure 3

Relative configurations of Chl *a*611 and *a*612 and their cryo-EM maps. Chl *a*611 was overlayed to compare relative configuration of Chl *a*612 using Mg, NA, NB, NC, and ND atoms in its porphyrin rings. Both porphyrin rigs of the Chls and cryo-EM maps of C_2S_2, $C_2S_2M_2L_2$, and PSI–LHCI–LHCII are represented by pink, green, and purple colors, respectively.

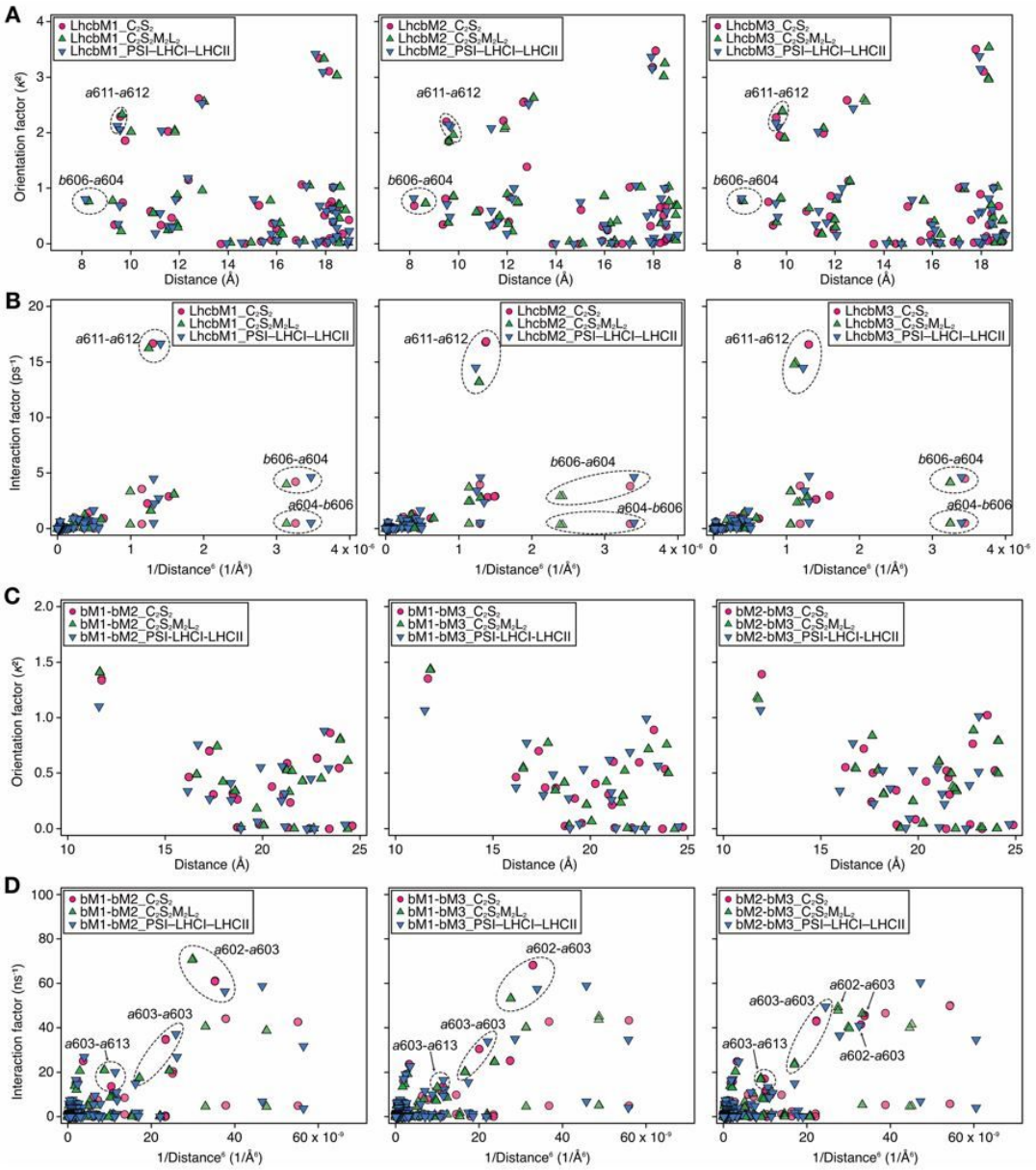

Figure 4

Configurational factors of Chls in LHCII trimers. (A) Scatter plots of configuration factors (Orientation factor and distance) between all Chls in each LhcbM subunit of each photosystem supercomplex. (B) Scatter plots of interaction factor (Energy transfer rate based on the FRET principle) and 1/distance^6 derived from (A). (C) Scatter plots of the configuration factors between Chls mediating inter-LHCII energy transfer (LhcbM1-LhcbM2, bM1-bM2; LhcbM1-LhcbM3, bM1-bM3; LhcbM2-LhcbM3, bM2-bM3) in the LHCII trimer of each photosystem supercomplex. (D) Scatter plots of interaction factors and 1/distance^6 derived from (A). C_2S_2, $C_2S_2M_2L_2$, and PSI–LHCI–LHCII are represented by pink, green, and cyan colors, respectively.

Supplementary Files

This is a list of supplementary files associated with this preprint. Click to download.

- LHCIIConformationsupEK220117.pdf